Enhancing Hydride Thermodynamics Through Nanostructuring

Jennifer Wilcox, Assistant Professor, Energy Resources Engineering;

Abstract

The phase stability diagrams for the decomposition of magnesium alanate [$Mg(AlH_4)_2$] nanoparticles were constructed as a function of particle size and temperature to better understand nanostructuring of the complex hydrides for hydrogen storage. Relatively smaller nanoparticles of $Mg(AlH_4)_2$, MgH_2, Al, and Mg ranging from 1 to 2 nm were directly calculated by using density functional theory (DFT) calculations, and cluster expansion and Monte Carlo simulation methods were developed to predict the phase stabilities of 2-100 nm nanoparticles. Our prediction demonstrates that bulk $Mg(AlH_4)_2$ can release hydrogen but its uptake reaction is unfavorable, and bulk $Mg(AlH_4)_2$ is metastable with respect to bulk MgH_2. However, in the cases of nanoparticle systems, hydrogen release and its recharging may be possible by controlling the particle size and temperature, which may facilitate experimental studies to determine the thermodynamically favored reaction pathways for the dehydrogenation and hydrogenation processes of $Mg(AlH_4)_2$ nanoparticles. We also provide the equilibrium diagrams for $Mg(AlH_4)_2$ nanoparticle decomposition depending on a hydrogen partial pressure.

Introduction

Metal hydrides have recently attracted interest as hydrogen storage materials for transportation applications.[1,2] In particular, magnesium hydride (MgH_2) has gained a great deal of attention due to its high gravimetric and volumetric storage capacities, i.e., 7.6 wt. % H_2 and 111 kg H_2/m^3, respectively.[1-3] Although MgH_2 requires a high temperature to release H_2 due to its high heat of formation, this may be overcome by adding Si to form Mg_2Si; however, the hydrogenation reaction (i.e., the reverse reaction of releasing H_2) has not been shown to readily occur, even at pressures up to 100 bar of H_2 and at a temperature of 150 °C.[4] This is likely in part due to kinetically unfavorable H_2 dissociation on the Mg_2Si surface.[5]

In addition to the Mg-based metal hydrides, complex hydrides including alanates ($[AlH_4]^-$) have recently gained attention as alternative hydrogen storage materials. Examples include $NaAlH_4$, $LiAlH_4$, $KAlH_4$, $Mg(AlH_4)_2$, Na_3AlH_6, Li_3AlH_6, and Na_2LiAlH_6.[6,7] Many of these materials have been known to release H_2 upon contact with water with highly irreversible hydrolysis reactions, a process known as "one-pass" hydrogen storage. [6,7] For example, $Mg(AlH_4)_2$ can exothermically dehydrogenate at 163^{0}C, but its direct rehydrogenation is not thermodynamically favorable. [8] As another example, $LiAlH_4$ shows similar kinetic and thermodynamic barriers when it is rehydrogenated. The first dehydrogenation of $LiAlH_4$ is an exothermic process with an approximate ΔH of –10 kJ/(mol of H_2), [9] but its reverse process proceeds endothermically with ΔH of 9 kJ/(mol of H_2) by which direct hydrogenation does not occur.

To overcome the kinetic limitation to reversibility of hydrogenation process, alanates doped with titanium have been suggested not only to achieve kinetically enhanced dehydrogenation, but also to make the process reversible.[10] For example, the reversible dehydrogenation of $LiNa_2AlH_6$ to LiH, 2NaH, and Al could be achieved by doping Ti

with the complex hydride.[10] Another well-known method for overcoming the kinetic barriers in the hydrogenation of complex hydrides is nanostructuring and nanocatalysis.[11]A DFT-based theoretical study, for example, showed that as the MgH_2 cluster size decreases below 19 Mg atoms, MgH_2 becomes more destabilized, resulting in a significantly lower hydrogen desorption energy.[12] An experimental study also found that upon size restriction of nanoparticles of $NaAlH_4$, $LiAlH_4$, and $LiBH_4$, a drastic enhancement of the hydrogen desorption properties can be achieved.[13]

In nanoparticles of complex hydrides, predicting what phases would be more stable as a function of nanoparticle size may facilitate the rational design of nanostructured complex hydrides for hydrogen storage. In the current work, as a starting point toward understanding reversible dehydrogenation and rehydrogenation process of the complex hydrides, we construct a phase stability diagram of $Mg(AlH_4)_2$ nanoparticles as a function of particle size and temperature. For this, the following three steps were conducted: i) first-principles calculations for total energies of a series of configurations of complex hydride nanoparticles, ii) construction of a cluster expansion parameterized by the total energies calculated in step i), which enables rapid calculation of the total energy as a function of particle size and shape, and iii) thermodynamics predictions equipped with the cluster expansion-calculated properties of nanoparticles to calculate equilibrium phase boundaries.

Methodology

Nanoparticle decomposition depends on the composition and the size of the reaction products. To evaluate the energy of the reaction products as a function of nanoparticle size, we first directly determined the electronic structures and energies of a series of configurations of fully relaxed nanoparticles [$Mg(AlH_4)_2$, MgH_2, Al, and Mg] with diameters up to ~2.3 nm by using density functional theory (DFT) calculations.[14,15] DFT calculations were performed by using the Vienna *Ab initio* Simulation Package (VASP)[16-19] with the projector-augmented wave (PAW)[20,21] method. The Perdew and Wang (PW91) [22] generalized gradient approximation (GGA) exchange-correlation functional was used. A kinetic energy cutoff of 250 eV was used with a plane-wave basis set. The integration of the Brillouin zone was conducted at the Γ-point using first-order Methfessel-Paxton smearing[23] with a width of 0.2 eV.

Based on the DFT-calculated energies and structures of the nanoparticles, we employed the cluster expansion-based approach employed by Mueller and Ceder[24] to predict the free energies of larger nanoparticles with diameters up to 100 nm. In this approach, the structure of the particle is represented on a lattice of sites, where each site can be either occupied or vacant. Site variables are assigned to each site, where the variable takes a value of +1 for an occupied site and -1 for a vacant site. The total energy of a nanoparticle configuration is then expanded as linear combination "cluster functions" as shown in Eq. (1).

$$E(\mathbf{s}) = \sum_{clusters} V_{cluster} \prod_{i \in cluster} s_i \qquad (1)$$

where **s** is the set of all site variables and s_i represents the site variable for the i^{th} site. $V_{cluster}$ are unknown expansion coefficients known as effective cluster interactions (ECI), which were determined by fitting to a training set of the DFT-calculated energies and structures. For Mg $(AlH_4)_2$ nanoparticles, we assigned a single site to each AlH_4 anion, due to relatively strong Al–H bonds as depicted in Figure 1. During structural relaxation the atoms will typically move from their original sites (Figure 2), and the energies of the relaxed structures were used to parameterize the cluster expansion. It was assumed that the nanoparticles were charge-balanced systems assigning oxidation states of Mg^{2+}, Al^{3+}, and H^{1-} to $Mg(AlH_4)_2$. Details of the cluster expansion and its validation are discussed in reference 24 where a similar approach was used to construct phase diagrams for sodium alanate ($NaAlH_4$) nanoparticles.

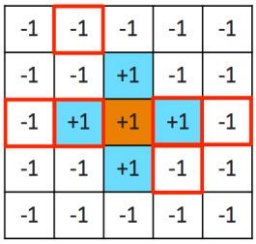

Figure 1. Schematic representation of a cluster expansion for a $Mg(AlH_4)_2$ nanoparticle in a 2-dimensional box. Orange, blue, and white sites are occupied by Mg, AlH_4, and vacuum, respectively. The spin variables of Mg and AlH_4-occupied sites are +1, and the variables of vacuum sites are –1. Clusters of a single site, a nearest-neighbor pair of sites, and a triplet of sites are represented in red.

Gibbs free energies of the Al–H–Mg nanoparticles [$G(n,T)$] can be described as a function of particle size (n) and temperature (T) in Eq. (2) ~ (4).

$$G(n,T) = G_{bulk}(T) + E_{form}(n) \tag{2}$$

$$G_{bulk}(T) = a + bT + cT\ln T + dT^2 + eT^3 + f/T + \sum_i g_i T^i \tag{3}$$

$$E_{form}(n) = (E_{particle} - E_{bulk} \times n)/n \tag{4}$$

where $G_{bulk}(T)$ represents the Gibbs free energy of the pure elements (bulk) and $E_{form}(n)$ is the formation energy of nanoparticle relative to bulk per formula unit. n represents the number of formula units, a to f and g_i are coefficients, and i indicates a set of integers. $E_{particle}$ and E_{bulk} represent the total energy of a nanoparticle and a bulk formula unit, respectively. $G_{bulk}(T)$ of the Al–H–Mg nanoparticles are well described by Palumbo et al.[25] Formula units of bulk $Mg(AlH_4)_2$, MgH_2, Al, and Mg are $Mg_1Al_2H_8$, Mg_2H_4, Al_1, and Mg_2, respectively.

Results

Figure 2 shows the molar formation energies (E_{form}) of Al and $Mg(AlH_4)_2$ nanoparticles calculated based on respective training sets of 50 ~ 200 and 13 ~ 50 formula units. The cluster expansion predicts the formation energies up to 1,600 and 450 formula units of Al and $Mg(AlH_4)_2$ nanoparticles, respectively. The molar formation energies approach zero

as the particle size increases up to bulk. The fitted equations are used for the prediction of the formation energies of nanoparticles up to 100 nm by using Eq. (2) and (3). Although there is discrepancy between the calculated ones and the fitted equations especially for relatively smaller particle sizes, the difference in the molar formation energy converges close to zero with increasing the particle sizes. Similar plots for Mg and MgH_2 are shown in the Supplementary Information, Figure S1. The resulting E_{form} terms for Al, $Mg(AlH_4)_2$, Mg, and MgH_2 are $268.25n^{-0.413}$, $204.06n^{-0.406}$, $1071.5n^{-0.673}$, and $137.10n^{-0.156}$, respectively.

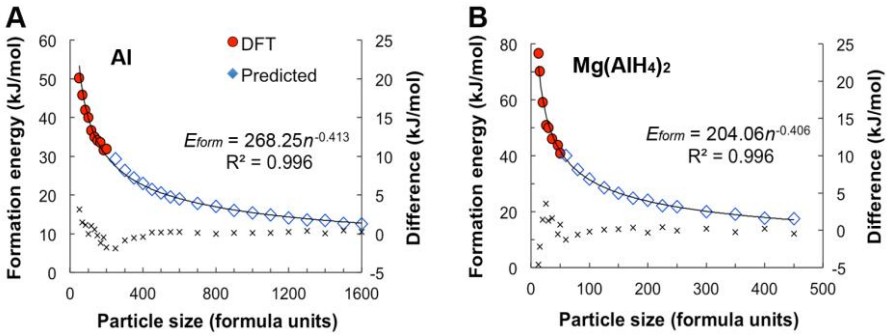

Figure 2. DFT-calculated (circles) and cluster expansion-predicted (diamonds) formation energies relative to bulk for (A) Al and (B) $Mg(AlH_4)_2$ nanoparticles. The solid lines indicate fitted formation energies (left scale). The secondary y-axis represents difference ('×' markers) between the fitted equation and the calculated or predicted data (right scale).

$Mg(AlH_4)_2$ compounds decomposes in two steps as shown in Eq. (5) and (6).[25-27] Alternatively, the reaction (6) may proceed in two sequential reactions as shown in Eq. (7) and (8) depending on the completion of the Al_3Mg_2 formation reaction.[26] Also, an intermediate metastable $MgAlH_5$ compound can be formed during the decomposition of $Mg(AlH_4)_2$ by reacting with excessive activated MgH_2.[28] In the current work, we focus on comparing the phase stability of $Mg(AlH_4)_2$ [Eq. (5)] and MgH_2 [Eq. (7)] between bulk and nanoparticle phases due to the complexity of the unit cell structure of Al_3Mg_2 consisting of 1,871 atoms.

$$Mg(AlH_4)_2 \rightarrow MgH_2 + 2Al + 3H_2 \quad (5)$$

$$MgH_2 + 2Al \rightarrow \tfrac{1}{2}Al_3Mg_2 + \tfrac{1}{2}Al + H_2 \quad (6)$$

$$MgH_2 \rightarrow Mg + H_2 \quad (7)$$

$$Mg + 2Al \rightarrow \tfrac{1}{2}Al_3Mg_2 + \tfrac{1}{2}Al \quad (8)$$

The resulting Gibbs free energy changes [$\Delta G(n,T)$] for the decomposition reactions of $Mg(AlH_4)_2$ [Eq. (5)] and MgH_2 [Eq. (7)] are given as a function of particle size (n) and temperature (T) in the unit of kJ/mol formula unit assuming a hydrogen partial pressure of 101,325 Pa (Figure 3 and 4, respectively). Note that for every n units of $Mg(AlH_4)_2$, there are $2n$ units of Al, n units of Mg, and n units of MgH_2, resulting in the n variables of the E_{form} terms for $Mg(AlH_4)_2$, Al, Mg, and MgH_2 should be n, $2n$, n, and n when calculating $\Delta E_{form}(n)$ in the $\Delta G(n,T)$ calculations. The particle diameter (in nm) was

related to the number of formula units (n) by employing Eq. (9), which is derived from the relationship between n and the experimentally determined $NaAlH_4$ nanoparticle size.[24,29]

$$d = \sqrt[3]{0.0716958n} \quad (9)$$

Figure 3 shows the phase stability diagrams for bulk and nanoparticle phases of $Mg(AlH_4)_2$ decomposition [Eq. (5)] as a function of the particle size (nm) and temperature. To predict the bulk phases, the $\Delta E_{form}(n)$ terms were omitted. In the case of bulk (Figure 3A), ΔG is negative at temperatures ranging from 0 to 200°C, indicating that the decomposition of $Mg(AlH_4)_2$ is favorable but the reaction is irreversible (i.e., the reaction of Eq. (5) always proceeds from the left to the right side). This observation agrees with the DFT works of Palumbo *et al*.[25] in that no stable phase of bulk $Mg(AlH_4)_2$ appears in a pressure-temperature equilibrium diagram for bulk $Mg(AlH_4)_2$. Fichtner *et al*.[8] also experimentally demonstrated that $Mg(AlH_4)_2$ can exothermically dehydrogenate at 163^0C but it is thermodynamically irreversible reaction. Our results support the conclusion that that bulk $Mg(AlH_4)_2$ is not suitable as a reversible hydrogen storage material.[26]

For very small nanoparticles, the formation energy becomes positive as the particle size and temperature decreases (Figure 3B). The positive ΔG region indicates the formation of $Mg(AlH_4)_2$. The temperatures and particle sizes at which ΔG is equal to zero, and hence dehydrogenation is reversible, are shown in Figure 3C. This suggests that hydrogen release and its recharging may be possible by controlling the particle size and temperature. For example, in Figure 3C if the nanoparticle sizes are kept to be around 4 nm, hydrogen can be released when temperature increases above around 100 °C and can be stored when temperature decreases below 100 °C. The reason $Mg(AlH_4)_2$ is predicted to become relatively more stable at small particle sizes is that the even smaller MgH_2 and Al nanoparticles it decomposes into would be destabilized by their higher surface / volume ratio.

Similarly, Figure 4 shows the phase stability diagrams for bulk and nanoparticle phases of MgH_2 decomposition [Eq. (7)] as a function of the particle size (nm) and temperature. The free energy of formation (ΔG) is positive at temperatures up to 200 °C, indicating that the hydrogen release from MgH_2 is unlikely at these temperatures; (Figure 4A). Together with the fact of bulk $Mg(AlH_4)_2$ as shown in Figure 3A (i.e., the exothermic and endothermic decompositions of bulk $Mg(AlH_4)_2$ and MgH_2, respectively), it is concluded that bulk $Mg(AlH_4)_2$ is metastable with respect to bulk MgH_2.[25] However, the MgH_2 nanoparticle system can show negative ΔG as the particle size decreases and temperature increases in Figure 4B. The negative ΔG region indicates the decomposition of MgH_2, releasing hydrogen. For example, in Figure 4C where the line of $\Delta G = 0$ indicates the nanoparticle phase boundary, if the nanoparticle sizes are kept to be around 15 nm, hydrogen can be released when temperature increases above around 100 °C and can be stored when temperature decreases below 100 °C.

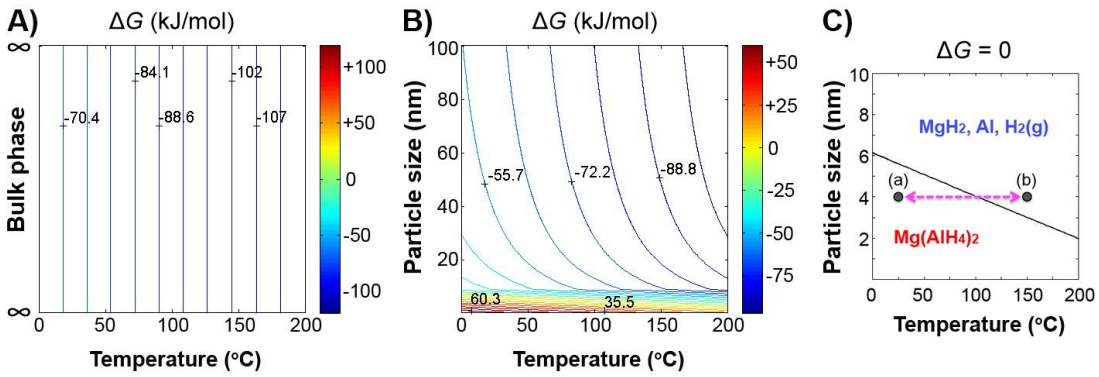

Figure 3. Phase stability diagrams for bulk (A) and nanoparticle (B) phases of $Mg(AlH_4)_2$ decomposition [Eq. (5)] as a function of the particle size (nm) and temperature under the pressure of 101,325 Pa. (C) Equilibrium diagrams of the nanoparticle decomposition with a line of $\Delta G = 0$. Arrows with (a) and (b) indicate examples of temperature change.

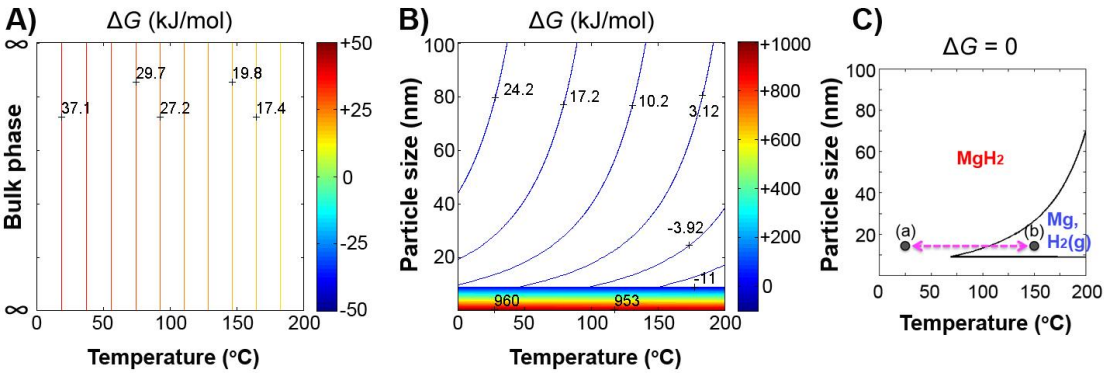

Figure 4. Phase stability diagrams for bulk (A) and nanoparticle (B) phases of MgH_2 decomposition [Eq. (7)] as a function of the particle size (nm) and temperature under the pressure of 101,325 Pa. (C) Equilibrium diagrams of the nanoparticle decomposition with a line of $\Delta G = 0$. Arrows with (a) and (b) indicate examples of temperature change.

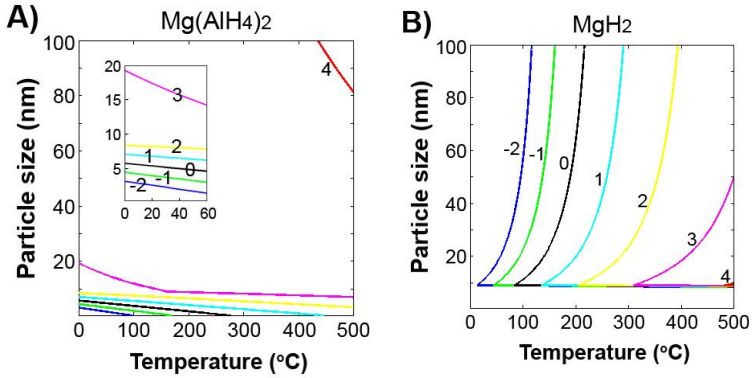

Figure 5. Equilibrium diagrams of $Mg(AlH_4)_2$ (A) and MgH_2 (B) decomposition depending on hydrogen partial pressure (P) in terms of $\log_{10}(P/P_0)$ where P_0 is the standard pressure of 101,325 Pa. An inset in (A) represents magnified region outlined by T = 0 to 60 °C and n = 0 to 20 nm.

The hydrogen partial pressure may influence the thermodynamics of $Mg(AlH_4)_2$ and MgH_2 decomposition. To examine this, the hydrogen partial pressure was varied from $101{,}325\times10^{-2}$ to $101{,}325\times10^{4}$ Pa under the temperature ranges up to 500 °C[25] where the phase stability of bulk $Mg(AlH_4)_2$ was previously examined. As shown in Figure 5, the phase regions of $Mg(AlH_4)_2$ and MgH_2 are enlarged as the pressure increases, whose trend fairly agrees with *ab initio*-based thermodynamics predictions for the phase stability of bulk $Mg(AlH_4)_2$ depending on temperature and pressure.[25] In the case of $Mg(AlH_4)_2$ nanoparticle, by increasing the pressure it may be beneficial that larger nanoparticles may show the same behavior of hydrogen release and uptake compared to that of smaller ones at a certain temperature range, which may reduce technical problems associated with the synthesis of smaller nanoparticle below approximately 5 nm. On the other hand, MgH_2 nanoparticle shows the opposite behavior in the relationship between the pressure and the particle size; the lower the pressure, the larger the nanoparticle size at which the reaction is reversible at a fixed temperature.

Conclusion

The limitation of the current work lies in excluding the formation of an intermediate species of Al_3Mg_2 during the $Mg(AlH_4)_2$ decomposition, assuming the zero-point energy and entropy per formula unit for the nanoparticle was equivalent to that of the bulk materials, and estimating the relationship between the number of formula unit (n) and the experimentally determined nanoparticle sizes. Despite these limitations, the current work clearly demonstrates the difference in the behavior of hydrogen release and uptake between bulk and nanoparticle phases. The observations from the phase stability diagrams of the nanoparticles may provide useful insights to determine the pressure and nanoparticle sizes for the optimal hydrogen release and recharge on $Mg(AlH_4)_2$ nanoparticles.

References

(1) Kelly, S. T.; Van Atta, S. L.; Vajo, J. J.; Olson, G. L.; Clemens, B. M., Kinetic limitations of the Mg(2)Si system for reversible hydrogen storage. *Nanotechnology* **2009,** *20*, (20), 204017.

(2) Paskevicius, M.; Sheppard, D. A.; Chaudhary, A.-L.; Webb, C. J.; Gray, E. M.; Tian, H. Y.; Peterson, V. K.; Buckley, C. E., Kinetic limitations in the Mg-Si-H system. *International Journal of Hydrogen Energy* **2011,** *36*, 10779-10786.

(3) Kelekar, R.; Giffard, H.; Kelly, S. T.; Clemens, B. M., Formation and dissociation of MgH2 in epitaxial Mg thin films. *Journal of Applied Physics* **2007,** *101*, (11), 114311.

(4) Vajo, J. J.; Mertens, F.; Ahn, C. C.; Bowman, R. C.; Fultz, B., Altering hydrogen storage properties by hydride destabilization through alloy formation: LiH and MgH2 destabilized with Si. *Journal of Physical Chemistry B* **2004,** *108*, (37), 13977-13983.

(5) Dai, B.; Sholl, D. S.; Johnson, J. K., First-principles investigation of adsorption and dissociation of hydrogen on Mg2Si surfaces. *Journal of Physical Chemistry C* **2007,** *111*, (18), 6910-6916.

(6) Orimo, S. I.; Nakamori, Y.; Eliseo, J. R.; Zuttel, A.; Jensen, C. M., Complex hydrides for hydrogen storage. *Chem. Rev.* **2007,** *107*, (10), 4111-4132.

(7) Sakintuna, B.; Lamari-Darkrim, F.; Hirscher, M., Metal hydride materials for solid hydrogen storage: A review. *International Journal of Hydrogen Energy* **2007,** *32*, 1121-1140.

(8) Fichtner, M.; Fuhr, O.; Kircher, O., Magnesium alanate - a material for reversible hydrogen storage? *J. Alloy. Compd.* **2003,** *356*, 418-422.

(9) Block, J.; Gray, A. P., *Inorganic Chemistry* **1965,** *4*, (3), 304.

(10) Bogdanović, B.; Schwickardi, M., Ti-doped alkali metal aluminium hydrides as potential novel reversible hydrogen storage materials. *J. Alloy. Compd.* **1997,** *253*, 1-9.

(11) Pasquini, L.; Callini, E.; Piscopiello, E.; Montone, A.; Antisari, M. V.; Bonetti, E., Metal-hydride transformation kinetics in Mg nanoparticles. *Applied Physics Letters* **2009,** *94*, (4), 041918.

(12) Wagemans, R. W. P.; van Lenthe, J. H.; de Jongh, P. E.; van Dillen, A. J.; de Jong, K. P., Hydrogen storage in magnesium clusters: Quantum chemical study. *Journal of the American Chemical Society* **2005,** *127*, (47), 16675-16680.

(13) Christian, M.; Aguey-Zinsou, K.-F., Destabilisation of complex hydrides through size effects. *Nanoscale* **2010,** *2*, (12), 2587-2590.

(14) Hohenberg, P.; Kohn, W., Inhomogeneous Electron Gas. *Physical Review* **1964,** *136*, (3B), B864-B871.

(15) Kohn, W.; Sham, L. J., Self-Consistent Equations Including Exchange and Correlation Effects. *Physical Review* **1965,** *140*, (4A), A1133-A1138.

(16) Kresse, G.; Hafner, J., Ab initio molecular dynamics for liquid metals. *Physical Review B* **1993,** *47*, (1), 558-561.

(17) Kresse, G.; Hafner, J., Ab initio molecular-dynamics simulation of the liquid-metal amorphous-semiconductor transition in germanium. *Physical Review B* **1994,** *49*, (20), 14251-14269.

(18) Kresse, G.; Furthmüller, J., Efficient iterative schemes for ab initio total-energy calculations using a plane-wave basis set. *Physical Review B* **1996,** *54*, (16), 11169-11186.

(19) Kresse, G.; Furthmüller, J., Efficiency of ab-initio total energy calculations for metals and semiconductors using a plane-wave basis set. *Computational Materials Science* **1996,** *6*, (1), 15-50.

(20) Blöchl, P. E., Projector augmented-wave method. *Physical Review B* **1994,** *50*, (24), 17953-17979.

(21) Kresse, G.; Joubert, D., From ultrasoft pseudopotentials to the projector augmented-wave method. *Physical Review B* **1999,** *59*, (3), 1758-1775.

(22) Perdew, J. P.; Wang, Y., Accurate and simple analytic representation of the electron-gas correlation energy. *Physical Review B* **1992,** *45*, (23), 13244-13249.

(23) Methfessel, M.; Paxton, A. T., High-precision sampling for Brillouin-zone integration in metals. *Physical Review B* **1989,** *40*, (6), 3616-3621.

(24) Mueller, T.; Ceder, G., Effect of Particle Size on Hydrogen Release from Sodium Alanate Nanoparticles. *Acs Nano* **2010,** *4*, (10), 5647-5656.

(25) Palumbo, A.; Torres, F. J.; Ares, J. R.; Pisani, C.; Fernandez, J. F.; Baricco, A., Thermodynamic and ab initio investigation of the A1-H-Mg system. *Calphad-Computer Coupling of Phase Diagrams and Thermochemistry* **2007,** *31*, (4), 457-467.

(26) Kim, Y.; Lee, E. K.; Shim, J. H.; Cho, Y. W.; Yoon, K. B., Mechanochemical synthesis and thermal decomposition of Mg(AlH4)(2). *J. Alloy. Compd.* **2006,** *422*, (1-2), 283-287.

(27) Varin, R. A.; Chiu, C.; Czujko, T.; Wronski, Z., Mechano-chemical activation synthesis (MCAS) of nanocrystalline magnesium alanate hydride Mg(AlH4)(2) and its hydrogen desorption properties. *J. Alloy. Compd.* **2007,** *439*, (1-2), 302-311.

(28) Dymova, T. N.; Mal'tseva, N. N.; Konoplev, V. N.; Golovanova, A. I.; Aleksandrov, D. P.; Sizareva, A. S., Solid-phase solvate-free formation of magnesium hydroaluminates Mg(AlH4)(2) and MgAlH5 upon mechanochemical activation or heating of magnesium hydride and aluminum chloride mixtures. *Russian Journal of Coordination Chemistry* **2003,** *29*, (6), 385-389.

(29) Canton, P.; Fichtner, M.; Frommen, C.; Leon, A., Synchrotron x-ray studies of Ti-doped NaAlH4. *Journal of Physical Chemistry B* **2006,** *110*, (7), 3051-3054.

Contacts

Jennifer Wilcox: wilcoxj@stanford.edu